2022 International Symposium on Power Electronics,
Electrical Drives, Automation and Motion

Microcontroller based closed control-loop of an Interleaved Synchronous Buck Converter exploiting Monolithic GaN technology

Enrico Bottaro
University of Catania
Catania, Italy
enrico.bottaro@unict.it

Federica Cammarata
STMicroelectronics
Catania, Italy
federica.cammarata@st.com

Giuseppe Longo
STMicroelectronics
Catania, Italy
giuseppe-mos.longo@st.com

Gabriele Nicolosi
STMicroelectronics
Catania, Italy
gabriele.nicolosi@st.com

Santi Agatino Rizzo
University of Catania
Catania, Italy
santi.rizzo@unict.it

Filippo Scrimizzi
STMicroelectronics
Catania, Italy
filippo.scrimizzi@st.com

2022 International Symposium on Power Electronics, Electrical Drives, Automation and Motion (SPEEDAM) | 978-1-6654-8459-6/22/$31.00 ©2022 IEEE | DOI: 10.1109/SPEEDAM53979.2022.9842115

***Abstract*—Mild-hybrid market requires smart and flexible power conversion systems that dynamically adapt their behaviour according to the working conditions and operational needs. This sector also asks for high-efficient converters with limited dimension and weight. Optimal versatility and high power density can be achieved thanks to monolithic GaN technology. In this context, this paper presents a 48-12V interleaved conversion system based on the emerging GaN technology combined with a closed-loop control implemented using the STM32 microcontroller. The main feature of the proposed system is the dynamic closed-loop control implemented by the microcontroller that modulates the driving signals for the interleaved power stages at different load conditions. The microcontroller also introduces the important feature of overcurrent protection to increase the security level of the whole system and react in case of failure. The proposed system combines the improved switching behavior of the GaN compared to silicon and the interleaved synchronous structure to obtain 95% peak efficiency.**

Keywords— Gallium nitride, buck converter, interleaved converter, efficiency, mild hybrid, automotive, microcontroller, closed loop control, over current protection.

I. INTRODUCTION

The mild-hybrid sector represents a good compromise between the high cost of full-electric vehicles and the advantage introduced by the increasing electrification of transportation [1]. A mild hybrid solution requires power conversion systems with high efficiency and smaller size with high power density. High bandgap devices such as SiC and GaN are the best alternative to Silicon [2] for this application to achieve outstanding results. Lower switching losses allow to achieve higher switching frequency over the silicon limits, thus reducing heat sink dimension, the copper amount on the PCB layers and its size and finally the passive components' dimension with the relevant overall size of the system.

Mild-hybrid market requires intelligent and flexible systems that manage high currents. For a 48-12V DC/DC conversion system is required a current capability of over 50A [3] per phase up to 250A and an interleaved structure can be chosen to achieve these current values [4].

Closed-loop control by microcontrollers is a widely used technique for its simplicity and versatility. A microcontroller with a competitive cost can drive the power stage and it can adjust the signals by modulating their pulse width. This operation mode has been discussed in LED driving applications where the microcontroller is used to implement a closed-loop control to a proper LED brightness regulation [5].

Photovoltaic systems [6-9], or more complex ones in which the control chipsets the operation condition according to the application needs and produces bidirectional energy transfer systems [10] are other applications in which cheaper microcontrollers platforms can be used.

The innovative aspects introduced in this project are the use of the microcontroller for the closed-loop management of a high-frequency power conversion system, possible thanks to the use of GaN technology. An STM32 microcontroller, based on nucleo R401RE, dynamically adjusts the operating conditions of the power stage depending on the load conditions. This system includes some protective features to stop the driving stage in case of failure.

In Section II the design of the prototype, as well as the validation by simulation of the waveforms, to foresee the behavior in switching, is described. Section III deals with the driving stage and the control loop implementation. In Section IV the experimental setup, the tests and the measurements are reported.

II. DESIGN OF A MULTI-PHASE BUCK CONVERTER

In the following section, the validation of the design is carried out through a preliminary study by simulation is presented.

As known in the literature, the output voltage in a Buck converter can be ideally set to the desired value through the duty cycle D [11]. To improve the overall system efficiency is often used the synchronous rectification technique [12][13]. This solution replaces the diode with an active switch and it aims to reduce the losses associated with the conduction of the diode.

The synchronous rectification uses an active device that is driven in full conduction to reduce the losses due to the current flowing through it. For this reason and thanks to the bidirectionality of GaN device, it is possible to realize a synchronous structure using a monolithic e-mode GaN that replaces the freewheeling diode. In this way, the power dissipated during the conduction phase of the passive device can be expressed considering his R_{DSon}:

$$P_{switch\ on} = R_{DSon}\, I_{OUT}^2\, (1 - D) \qquad (1)$$

According to this structure, it is possible to realize the Buck topology using two active switches in a monolithic chip. A multi-phase interleaved structure provides better results in terms of overall conversion efficiency [1][14]. Therefore, a three-phase structure has been chosen, thus the converter

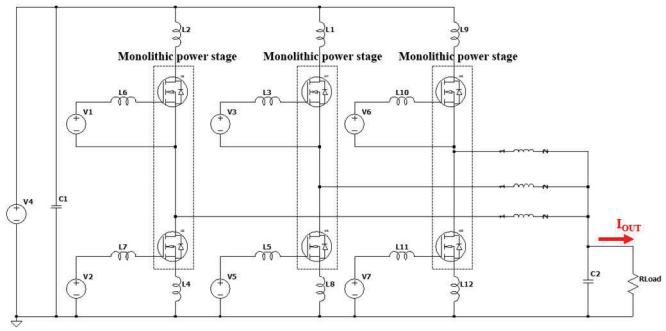

Figure 1: Schematic of a three-phase synchronous Buck converter

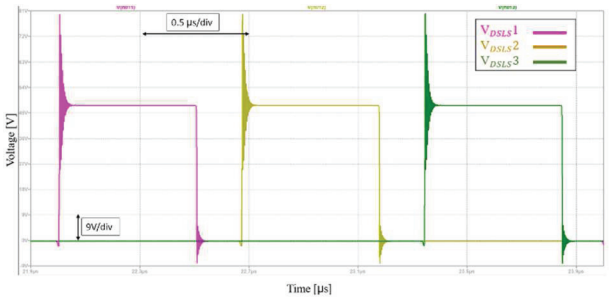

Figure 2: VDS of the low-side of each leg of the three-phase converter from simulation

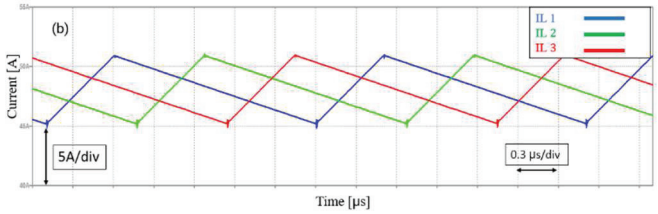

Figure 3: Current waveforms for each phase from simulation

consists of three monolithic devices that include high side and low side switches. This power stage is driven by a microcontroller and it can be schematized as shown in Fig. 1.

In the simulation, a spice HEMT GaN model with breakdown voltage equal to 100V, with proper $R_{DS(ON)}$ and Qg to match the power requirement of the application has been used. Some inductive contributions are also added to the basic schematic to emulate the stray parasitic inductive contributions of the layout. Figgs. 2 and 3 also report the voltage and current waveforms from simulation which highlight the theoretical operation of the three-phase system.

III. DRIVING WITH MICROCONTROLLER AND CONTROL LOOP

For the generation of PWM signals, four timers have been used among those available on the microcontroller. The three PWM signals required for the system need a phase shift of 120 degrees of the period. Considering the system working at a switching frequency of 500kHz it has been possible to calculate the necessary phase shift, at about 670 ns.

The phase shift required is very small and must be fixed with high precision to fix it stably. To achieve this precision, it has been necessary to use an auxiliary timer for synchronization purposes. The auxiliary timer has been set as a master to drive three other timers (slaves). Then, the three output logic signals have been sent from the microcontroller to the driving stage. The three logic signals generated by the microcontroller with the proper phase-shift are shown in Fig. 4.

The PWM signal used to drive the high side and low side pair is unique and externally generated by the microcontroller. The single PWM is firstly processed by a two-functions logical block. The first cleans up the PWM signal, at the input to the board, from possible noise that could disturb the high-frequency switching dynamics. The second one extracts from a single signal the two complementary driving signals for the high and low side switches to obtain synchronous commutation. In addition, the rising and falling edges of the two signals have been delayed by the dead time to avoid cross conduction phenomena inside the leg of the converter. The circuit consists of four NAND ports with Schmitt triggers 2 by 2 coupled to generate HI and LI logic signals. The dead-time circuit is represented in Fig. 5.

After the generation of the two logic signals, HI and LI are sent to the gate driver circuit. More specifically, the LMG1205 has been used to drive the high and low side of the monolithic GaN leg for synchronous rectification. It also integrates the diode necessary for the bootstrap circuit. A simplified application diagram of the realized system is reported in Fig. 6.

The closed-loop control has been implemented through the microcontroller is schematized in Fig. 7. The system starts to run when it receives the enable signal. In this first phase, the starting parameters for the shift of the timers and the amplitude of the duty cycle at no load are set.

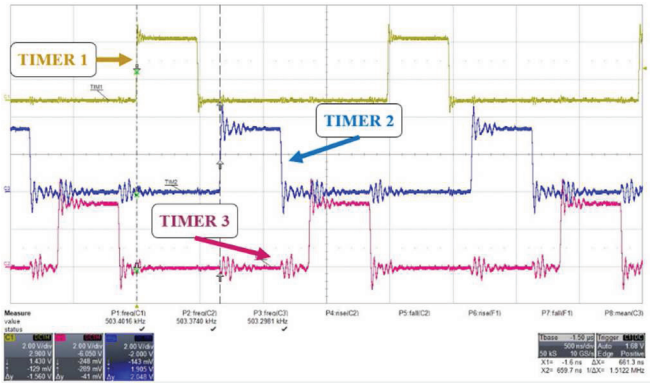

Figure 4: Logic output of the three timers from the microcontroller

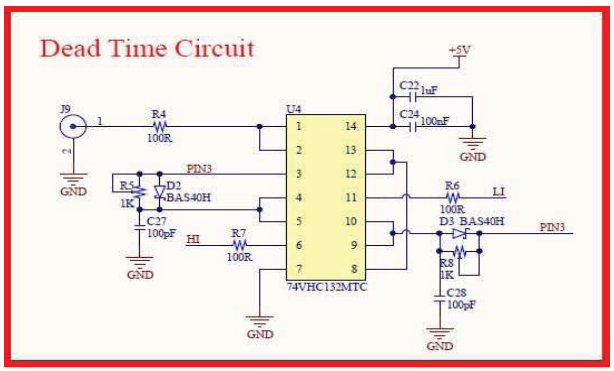

Figure 5: Altium schematic of the dead time circuit for each leg of the converter

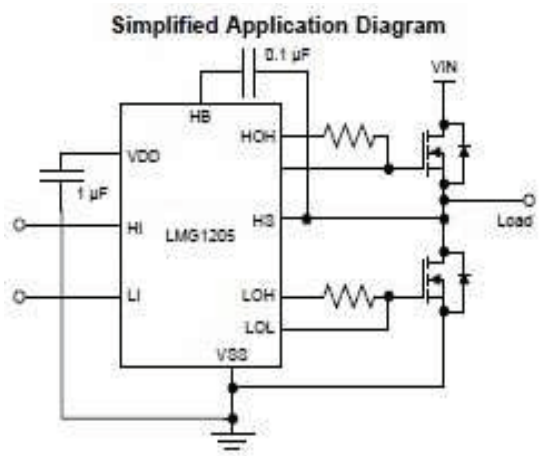

Figure 6: Simplified application diagram of gate driver connections for a single half-bridge

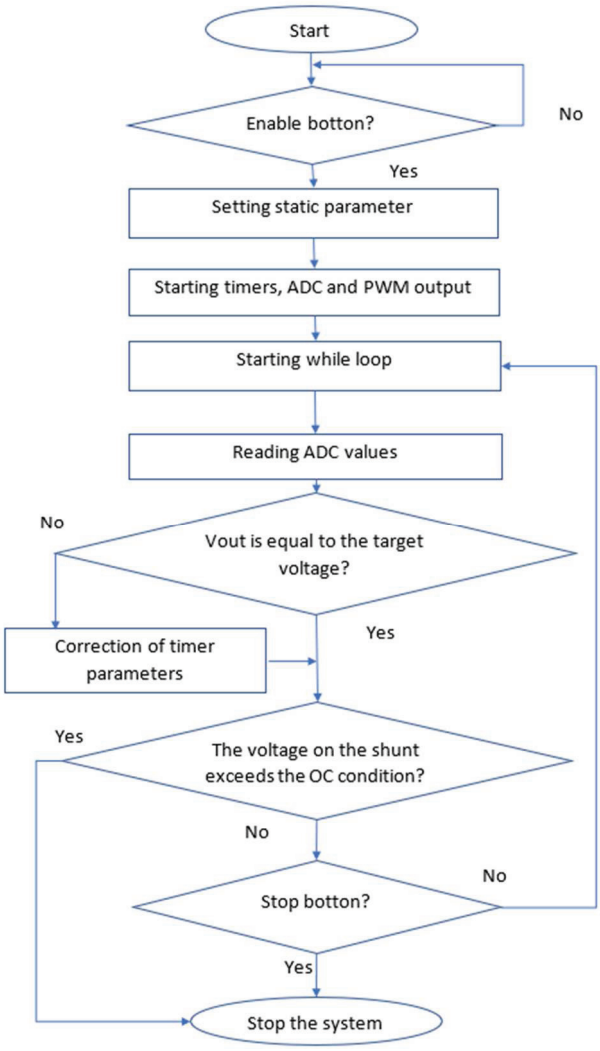

Figure 7: Flow diagram of the control loop performed by the microcontroller

The acquisition channels of the ADC are also started. The control loop is then started. The reading is performed on the voltage signals to achieve the appropriate actions: if the output signal is not equal to the established voltage target, the duty cycle regulation is performed; if the voltage across the shunt resistor exceeds a fixed threshold value the OC condition is detected and the system is stopped.

For this function, it has been necessary to enable the microcontroller to read, process and respond with a fast reaction to the system operation. The following two functions have been introduced for close-loop regulation. The duty cycle regulation modulates the amplitude of the PWM signals and keeps the output voltage constant at the desired value at different load conditions. The function of overcurrent protection (OCP) is to evaluate the phase current of the converter. It has been necessary the acquisition of five voltage signals from the converter to achieve these functions. The reading signal has been carried out by using the 12-bit digital/analog converters of the microcontroller set in continuous conversion mode.

For duty cycle regulation the output voltage of the converter must be taken for modulation of the on-time amplitude of the three phases. The output voltage is taken from a voltage divider with a 1:3 ratio, as reported in figure 8. A voltage buffer has been also used to decouple the input of the microcontroller from the power output.

The OCP feature is useful to maximize system security. This function allows stopping the system when a peak of current occurs due to a short circuit or a failure of some device. For the circuit reading on shunt resistance, the technique suggested in [15] has been implemented and tested. In this circuit topology, the voltage to the shunt resistor heads is sent to an operational amplifier that provides an output voltage that is used to drive a p-channel power MOSFET, used as a variable resistor. The modulation of the equivalent resistance involves a variation of the current that flows through the power switch. Then, it is possible to measure the voltage from the output of this circuit. The implemented circuit measures the voltage from the shunt resistor in Fig. 9, this voltage is then processed by the circuit in Fig. 10.

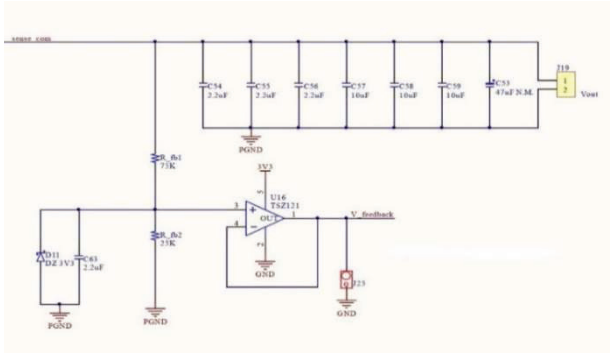

Figure 8: Altium schematic of the duty cycle regulation circuit

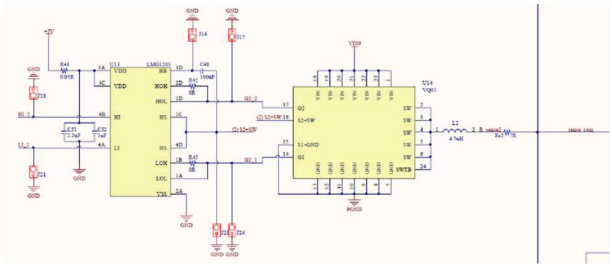

Figure 9: Altium schematic of the gate driver and power stage with a shunt resistor

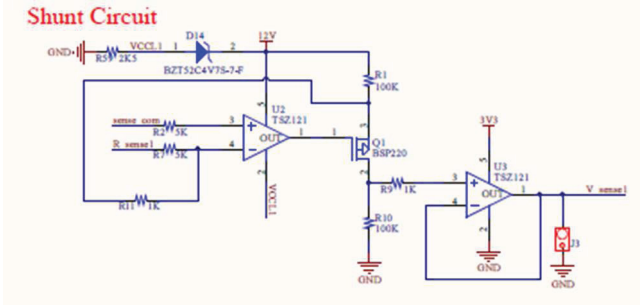

Figure 10: Altium schematic of shunt resistor sensing circuit

IV. EXPERIMENTAL VALIDATION

Experimental tests have been performed on the designed three-phase synchronous Buck prototype. Fig. 11 shows the top view of the prototype with the microcontroller. In this Section, the experimental setup and waveforms acquired during testing are reported. An efficiency evaluation is also shown.

a) Experimental setup

A test bench has been equipped with a 64 Xi 600 MHz Le Croy Oscilloscope and PP-005 Le Croy 500MHz passive probes to view the drain-source voltage and current waveforms. The Agilent 6012B DC Power Supply has been exploited to supply the gate driver's circuitry, while an active load is emulated by a Chroma 63101 DC Electronic Load. A Yokogawa WT210 Digital power meter has been used to estimate the power conversion efficiency, a Fluke 45 Dual Display Multimeter has been used to view the output voltage, GW INSTEK GPS-3303 power supply has been exploited to supply (Vin) the converter. To reduce the measurement oscillations and the deriving power losses due to inductive loops, the testing points have been designed to use passive probes equipped with pig tails ground contact. This particular type of probe minimizes the loop between the testing point of interest and the ground, and it is recommended for high-frequency applications.

The converter has been powered with two different voltages. A 12V power supply for logic and gate driver block and a 48V power supply for the power stage. In this case, the three PWM signals have been generated with an STM32 Nucleo 401RE microcontroller to make the system more versatile. The dead time has been generated through an appropriate dead time circuit realized with a 74VHC132 QUAD 2-INPUT SCHMITT NAND GATE. Two gate drivers LMG1205 have been used to drive the GaN half-bridge. The gate drivers must be placed as close as possible to the half-bridge devices to reduce the parasitic inductances and any interference that could be generated. The gate resistance has been set to zero to maximize the switching speed. The LC filter has been properly sized to reduce the output voltage oscillation: C = 36,6μF and L = 1 μH.

The measurements carried out show the V_{DS} of the low side of the converter legs and the three-phase currents. The output current at the common node was computed with a mathematical function of the oscilloscope.

a) Experimental results

The waveforms in Fig. 12 show the switching behavior of the system. The proper phase shift between each leg has been set through the microcontroller and it is highlighted by VDS waveforms for the low sides of each leg.

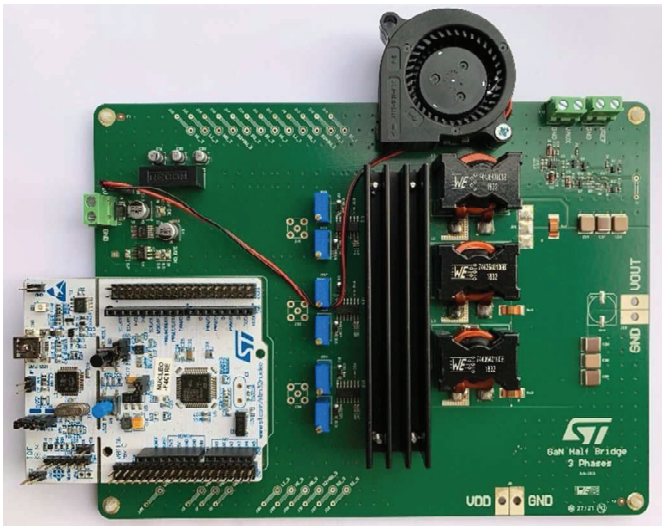

Figure 11: Top view of the testing board with the microcontroller and the converter

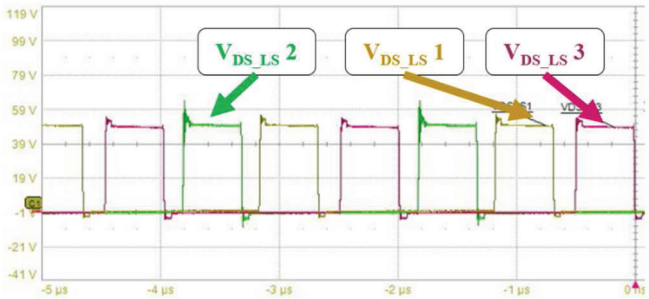

Figure 12: VDS for the low-side of each leg of three phase converter from developed board

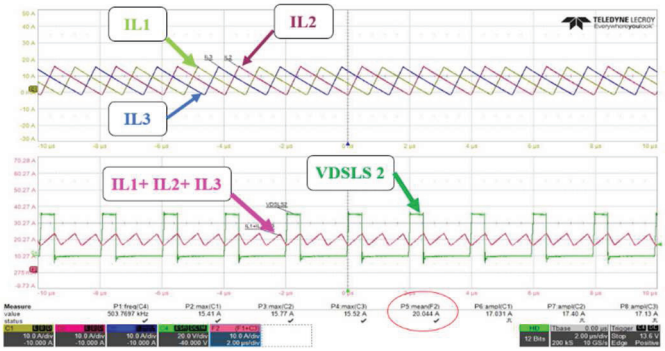

Figure 13: Phase current waveforms for each leg and total output current waveform at 20A load condition

From the waveforms, it is possible to observe the correct phase shift between the three phases and the interleaved operation. The measurements below show the switching frequency of the signals at the switch nodes, the duty cycles for each phase, the voltage peaks on V_{DS} signals. It is possible to observe that the second phase has voltage peaks higher than the other phases in zero load conditions.

Fig. 13 shows the three-phase currents, the voltage at the switch node for phase two and the total current at the common node of the three inductors expressed as the sum of the three currents. Two test conditions are reported: the first one with an output current of 20A; the second with an output current of 50A.

The system is perfectly balanced with a load current of 20A. The phase currents present the proper phase shift and the total current is divided into three legs. The average output current value can be visualized by the mean value of the mathematical function expressed by the sum of the three currents. The tests were also repeated for a load current of 50A. With a higher load, the spread on the threshold voltage value of the devices impacts more on the performance. This implies different current values for each phase, producing an imbalance in the distribution of the total current. This phenomenon is shown by the current waveforms in Fig. 14.

Output voltage regulation is a very important feature for conversion systems. It is important to ensure control over the output voltage in all operating conditions, both in the zero load and full load conditions. These two conditions are the most critical, especially for output capacitors. For this reason, it is necessary to perform fast the regulation, entrusted in this case to the microcontroller.

It is possible to report the complete system adjustment process with the three interleaved phases. As it can be seen from figures 15, 16 and 17 the microcontroller modulates the duty cycle of the drive signals to maintain the constant output voltage. The duty cycle starts from a value around 25,4% for the zero load condition, to a value around 25,9% for a load current of 30A and reaches a value around 26,4% for a load of 50A. It is necessary to underline that the output voltage is always fixed at a value of 12V highlighting the correct operation of the microcontroller.

The overcurrent protection function described has been tested on the application board. This function allows stopping the conversion in case of overcurrent condition ensuring a

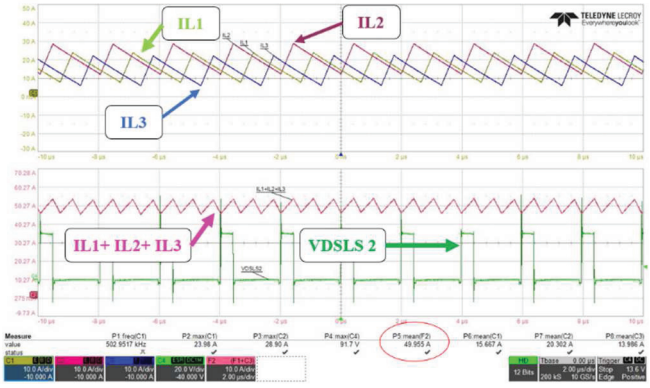

Figure 14: Phase current waveforms for each leg and total output current waveform at 50A load condition

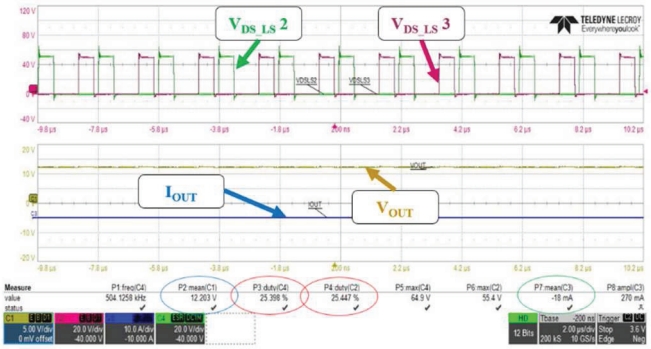

Figure 15: Duty cycle evaluation in zero load condition

safe condition for the system. The shunt resistor sensor circuit simulated have been tested on the evaluation boards at different loading condition. Therefore, it is possible to report the action of the microcontroller when an overcurrent condition is detected. Setting a threshold voltage value of 1.8V for Vsense, it is possible to observe how the microcontroller read the feedback voltage to detect the overcurrent event. Fig. 18 shows the current variation from 5A to 10A, V_{DS} signal for low side and V_{sense}.

The marked measurements show the Vsense and current values before and after the overcurrent condition. Waveforms show that the Vsense voltage exceeds the threshold set by the software and the microcontroller enables the shutdown after around 240 ms.

It was also possible to acquire data related to the overall efficiency of the developed system. The use of the three interleaved phases has allowed obtaining peak efficiency of 95% for current values between 20 and 30A.

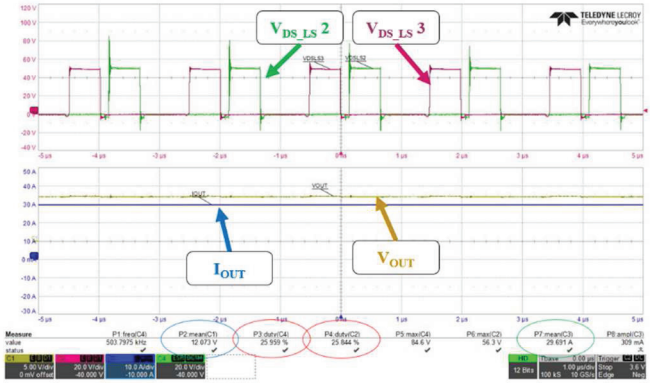

Figure 16: Duty cycle evaluation at 30A load condition

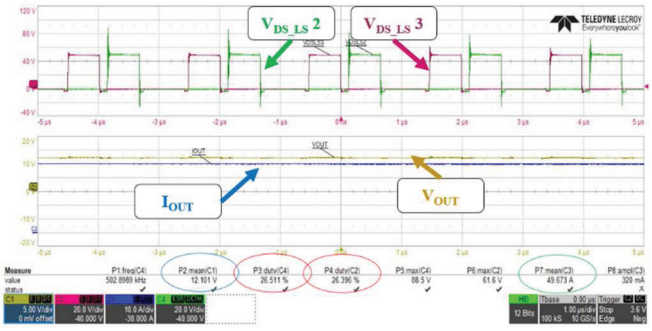

Figure 17: Duty cycle evaluation at 50A load condition

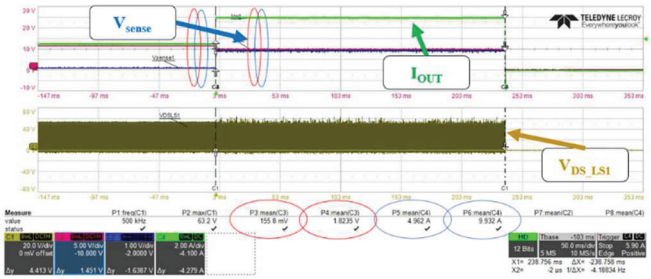

Figure 18: Overcurrent event and microcontroller intervention

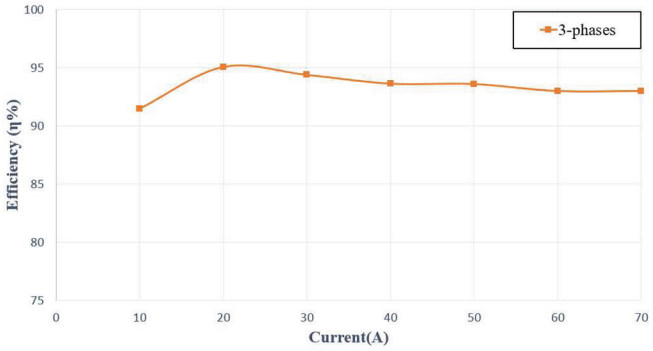

Figure 19: Efficiency curve of a three-phase interleaved system

V. Conclusion

An interleaved Buck converter adopting monolith GaN devices exploiting a closed-loop control based on a microcontroller has been presented. The innovative aspect is the control and management of the system through a microcontroller for the realization of the DC/DC 48-12V converter at 500kHz in monolith GaN technology. The combination of GaN solutions and microcontroller STM32 represents a new step toward the realization of high frequency and high-efficiency systems. The microcontroller has been used for both phase interleaving and closed-loop control. On this basis, several tests have been carried out to justify the use of interleaved solutions and the advantages of using GaN devices. These tests have shown that the microcontroller can effectively and independently manage the system, and the interleaved solutions allow to obtain improved efficiency also under low load conditions. Peak efficiency of 95% at a load condition of 25A with the three-phase system has been reached.

The conversion system has become more versatile thanks to the use of the microcontroller. The driving management of the phases has been carried out only by coding the microcontroller without the aid of external function generators. The microcontroller has, moreover, appropriately managed the regulation of the duty cycle of the phases and the detection of the overcurrent events. Starting from these features it has been possible to create a self-regulating system to keep the output at the target values.

Acknowledgment

The work has been supported in part by the project “Advanced power-trains and systems for full electric aircrafts - 2017MS9F49” funded by the “Ministero dell'Istruzione dell'Università e della Ricerca” under the call PRIN 2017.

References

[1] N. Keshmiri, D. Wang, B. Agrawal, R. Hou and A. Emadi, "Current Status and Future Trends of GaN HEMTs in Electrified Transportation," in IEEE Access, vol. 8, pp. 70553-70571, 2020.

[2] J. Ballestín-Fuertes, et al. “Role of Wide Bandgap Materials in Power Electronics for Smart Grids Applications,” Electronics, vol. 10, no. 6, p. 677, Mar. 2021.

[3] A. Emadi, S.S. Williamson, A. Khaligh, "Power electronics intensive solutions for advanced electric, hybrid electric, and fuel cell vehicular power systems," Tran. on Power El., vol. 21, no. 3, pp. 567-577, 2006.

[4] J. Zhang, J. -S. Lai, R. -Y. Kim and W. Yu, "High-Power Density Design of a Soft-Switching High-Power Bidirectional dc–dc Converter," Tran. on Power El., vol. 22, no. 4, pp. 1145-1153, 2007.

[5] I. Galkin, O. Tetervenoks, "The study of microcontroller based embedded system for smart lighting applications," *European Embedded Design in Educ. and Research Conf.*, 2014, pp. 105-108.

[6] S.M. Mukhtar, A.R.M. Saad, N. H. Hanafi, "A high efficiency microcontroller-based step-up push-pull DC-DC converter for PV inverter," Inter. Conference on Power and Energy, 2010, pp. 141-145.

[7] F. Chimento, S. Musumeci, A. Raciti, C. Sapuppo and M. Di Guardo, "A control algorithm for power converters in the field of photovoltaic applications," European Conference on Power Electronics and Applications, 2-5 Sept. 2007, Aalborg, Denmark, pp. 1-9.

[8] S. Foti et al., "An Optimal Current Control Strategy for Asymmetrical Hybrid Multilevel Inverters," in IEEE Transactions on Industry Applications, vol. 54, no. 5, pp. 4425-4436, Sept.-Oct. 2018

[9] D.Radianto, G.M.Dousoky, M.Shoyama, "Design and implementation of fast PWM boost converter based on low cost microcontroller for photovoltaic systems," IECON 2015, pp. 2324-2328.

[10] Y. Wu, Y. Wang and W. Ning, "Design of bidirectional DC-DC converter based on single chip microcomputer," 2018 Chinese Control And Decision Conference (CCDC), 2018, pp. 6004-6009.

[11] N. Mohan, T.M. Undeland, W.P. Robbins, “Power Electronics: Converters, Applications and Design”, John Wiley & sons, Inc. , 1995.

[12] Texas Instruments Incorporated, «Texas Instruments,» 2009. [Online – 7/4/2022]. Available: https://www.ti.com/lit/pdf/slyt358.

[13] F. Li, Y. Guan, Y. Wang, D. Xu, W. Wang, "A 20MHz Isolated Synchronous Rectification DC-DC Converter Based on GaN HEMT," IECON 2018, pp. 841-846.

[14] B. Li, et al., "A High Frequency High Efficiency GaN Based Bi-Directional 48V/12V Converter with PCB Coupled Inductor for Mild Hybrid Vehicle," WiPDA 2018, pp. 204-211.

[15] N. Aupetit, «STMicroelectronics – Application note » November 2016. [Online 7/4/2022]. Available: https://www.st.com/resource/en/application_note/dm00272583-highside-current-sensing-for-applications-using-high-commonmode-voltage-stmicroelectronics.pdf.